ELSEVIER

Applied Ocean Research 23 (2001) 63–81

Applied Ocean Research

www.elsevier.com/locate/apor

Dynamic tension in risers and mooring lines: an algebraic approximation for harmonic excitation

J.A.P. Aranha*, M.O. Pinto

Department of Naval Engineering, USP, CP61548, Sao Paulo, Brazil

Received 20 June 2000; revised 20 March 2001

Abstract

A riser or mooring line, when excited dynamically at its upper end, resists the imposed displacement by increasing its tension. Viscous damping in the lateral motion is known to be crucial and the resulting problem is thus intrinsically nonlinear. In this paper, an algebraic expression for the dynamic tension, formerly obtained [Polar Engineers, ISOPE'-93 (1993)], is revised and enlarged, once the variation of the tension along the suspended length is specifically focused here. The obtained expression is systematically compared with results from usual nonlinear time domain programs and with experiments, showing a fair agreement. This algebraic expression is used then, in two accompanying papers, to address relevant problems from a more practical point of view: in the first one, the question of the dynamical compression of risers, with a proper estimative of the related critical load, is analyzed in conjunction with the results here derived; in the second one, the algebraic expression is used to obtain an analytic approximation for the probability density function of the dynamic tension in random waves.

Keywords: Dyanamic tension; Risers; Algebraic approximation

1. Introduction

Consider a *cable*, whether it is a riser or a mooring line, hanging from a floating system and resting on the sea floor in the other end. The cable may be made by a junction of different materials, as it is usual in a mooring line configuration, or it may have some few concentrated buoys or weights or even it can also be exposed to the action of a steady ocean current in the cable's plane. If the flexural rigidity EJ is 'small', in the sense that its influence can be felt only in the boundary layers where the change in curvature is large, then the equilibrium of the cable can be determined assuming EJ = 0, see Ref. [3]. The static configuration is defined by the functions $\{\theta(s);T(s)\}$, where $\theta(s)$ is the angle between the tangent to the cable and the horizontal plane and $T(s)$ is the static tension. If l is the suspended length, the curvilinear coordinate of the point anchored in the floating system is $s = l$, $s = 0$ being the coordinate of the touchdown point.

Given the static configuration, suppose that a harmonic motion $U(t) = U_0\cos(\omega t)$ is imposed at the suspended end $s = l$, in the direction of the cable's tangent; it can be shown, see Section 4, that the displacement in the normal direction gives rise to a small correction in the tension and can therefore be ignored. The displacement $U(t)$ is due to the action of the sea wave on the floating body and the main objective of the present analysis is to determine the dynamic tension $\hat{T}_D(s,t)$ caused by such displacement.

From a numerical point of view, the problem is apparently straightforward, even more if it is observed that the large viscous damping in the lateral motion eliminates a possible resonant phenomenon. In spite of this, the dynamic tension can be very large: in fact, when either the amplitude U_0 of the displacement or the frequency ω increases, the viscous dissipation becomes so strong that the cable almost *freezes* in its equilibrium position. The imposed displacement is then absorbed elastically by the cable, see Ref. [9], giving rise to a large value of the tension. In fact, in this limit the *elastic tension* $T_e = EA(U_0/l + l')$ can be reached, where EA is the axial stiffness and l' is the *effective length* of the cable on the ground, see Section 2 for a proper definition; to get an idea about the possible level of tension, if $U_0 = 4$ m and $l + l' = 2000$ m the elastic strain $\epsilon_e = T_e/EA$ becomes equal to the steel yield strain.

There are thus two time scales in the problem, each one related to particular mechanisms for the reactive forces that can be best visualized in limit situations: if the cable is

* Corresponding author. Address: Department of Naval and Ocean Engineering, EPSUP, Cidade University, CEP 05508-900, Sao Paulo, Brazil. Tel.: +55-11-3818-5340; fax: +55-11-3818-5717.

E-mail address: japaran@usp.br (J.A.P. Aranha).

0141-1187/01/$ - see front matter
PII: S0141-1187(01)00008-6

loose, for example, it accommodates the imposed displacement by a geometric change in the catenary and the related time scale is associated with the cable's lateral frequency ω_c; on the other hand, a *tight* cable absorbs the imposed displacement elastically, with a time scale related to the elastic axial frequency ω_e. Obviously, these two time scales coexist in an actual problem and the numerical scheme has then to deal with discrepant time scales, since in general, as seen in Section 2, $\omega_e \gg \omega_c$. Discrepancy in time scales presents a natural difficulty for numerical integration, but this is not the only source of numerical problems in the analysis. In fact, the discrete system uses lumped masses that hits the ground in the vicinity of the touchdown point, giving rise to impact forces that are propagated along the cable. These impact forces are spurious, since they are caused by the discretization,[1] and they impose spurious high frequency components on the dynamic tension that are not very much attenuated along the cable, unless the axial damping is very high. Obviously, this effect diminishes as the mesh size becomes thinner, but for a typical mesh size the spurious tension, although small compared with T_e, can become noticeable when compared with the static tension, blurring then the signal of the total tension. One will have the opportunity to observe this phenomenon in the few simulations to be shown here and it is a matter of concern how to deal numerically with these higher harmonic components, observed also at the suspended end of the cable. Simply filtering them does not seem to be a wise solution since, though spurious in the continuum context, they are innate to the discrete models and, once excited, the higher harmonics interact nonlinearly, affecting the energy of the fundamental harmonic.

These critical remarks about the numerical solutions should be looked into a proper perspective: they do not imply that numerical results are useless and, as a matter of fact, numerical simulations have been extensively used, in the present paper and in the accompanying ones, as a reference for the analytic results. Although recognizing the usefulness of these solutions, with their numerical robustness and broad generality, the intention here was to draw the attention to some more subtle aspects of the cable dynamics that can be relevant in certain circumstances.

On the other hand, the same discrepant time scales that cause numerical trouble can be explored to obtain asymptotic solutions for the cable dynamics. The basic idea is motivated by the fact that, as seen in Section 2, the imposed frequency ω is of the order of magnitude of the cable's lateral frequency ω_c and so, in general, $\omega \ll \omega_e$. If now k is the axial wavenumber related to ω then, from the definition of the axial wave velocity, one has $c_e = \omega/k = \omega_e/k_e$, with $k_e \approx \pi/l + l'$ being the wavenumber of the first axial natural mode. It turns out that $k(l + l') \approx \pi(\omega/\omega_e) \ll 1$, showing that the natural length scale for the axial dynamic tension is much larger than the cable's length; in first approximation, then, *the dynamic tension can be assumed constant along the cable's length* and it can be obtained from the overall dynamic equilibrium of the cable. This is the basis of the algebraic approximation derived in Ref. [2] where, in essence, the dynamic equations are integrated along the suspended length to obtain a closed form expression for the dynamic tension.

However, one point was not satisfactory, mainly for an almost vertical riser: for these geometries the variation of the dynamic tension along the cable is indeed small, when compared to the reference tension T_e, but it can be appreciable when compared with either the static tension or the dynamic tension at the touchdown. From a more practical point of view, then, the variation of the dynamic tension along the cable must be evaluated and one of the purposes in the present work is to present such 'second order' correction. The other intention was to show, in a more systematic way, comparison with numerical results obtained with different programs, calling the attention to the observed discrepancies when they happen and commentating them; at the same time, both the numerical results and the algebraic expression are compared with a set of experimental results, disclosing some of the numerical misbehavior described above.

This paper has been organized with the objective to focus the attention on these issues, placing then in a secondary plane the mathematical derivation of the algebraic expression. For this reason, Section 2 presents directly, besides some definitions, the final algebraic expression for the dynamic tension, the discussion being restricted there to some simple physical arguments that can help to interpret the final result; Section 3 is dedicated to a more systematic comparison with experiments and numerical results, with some pertinent discussion of the results. Only in the Appendix the detailed mathematical derivation of the algebraic expression is addressed.

2. The algebraic expression for the dynamic tension

Consider a *cable* fixed at the floating system in a certain point S and touching the sea floor at a point O; if s is the curvilinear coordinate, with $s = 0$ at O and $s = l$ at S, then l is the suspended length of the cable. The *static configuration* is defined by the coordinates $(x(s);z(s))$ satisfying the geometric equations $dx/ds = \cos\theta(s)$; $dz/ds = \sin\theta(s)$, with $\theta(s)$ being the angle between the cable's tangent and the horizontal axis. Let q be the submerged weight per unit of length of the cable and $T(s)$ its static tension, with particular values defined below:

$$T_S = T(l), \qquad T_0 = T(0). \tag{2.1a}$$

[1] In fact, it can be shown (see Ref. [3]) that in the *continuous problem* the cable in general 'rolls' in the ground without striking it. This result is confirmed by the experiments, since the observed time record of the tension does not show any evidence of higher harmonics, even when the cable slackens; see Section 3 of this work.

Let also Δl be the length of the cable resting on the sea floor, that is, the distance between the anchor A and the touchdown point O, and μ the friction coefficient between the cable and the soil. If the length $T_0/\mu q$ is smaller than Δl then, obviously, the static tension is zero in the interval $-\Delta l \le s \le -T_0/\mu q$ and the *effective length* of the cable on the sea floor will be $T_0/\mu q$. Denoting by l' this length, and observing that the whole cable is stretched when $\Delta l < T_0/\mu q$, then

$$l' = \mathrm{Min}\{\Delta l; T_0/\mu q\}. \tag{2.1b}$$

The *effective length* enters in the problem through the definition of the *elastic tension* T_e. As seen in the Introduction, this tension appears at the 'freezing condition', where the imposed displacement is absorbed elastically by the cable in a *quasi-static* way; in this perspective, the definition given in Eq. (2.1b) seems to be the most natural one even for the dynamical problem, as discussed in Section 4.

The cable's curvature is defined by the function

$$\frac{\mathrm{d}\theta}{\mathrm{d}s}(s) = \frac{q}{T_S}\chi_1(s), \tag{2.2a}$$

where $\chi_1(s)$ is directly determined from the static configuration; as it is shown in Section 4, the lateral harmonic displacement $v(s)$ is, in first approximation, proportional to the curvature and so $v(s) \propto \chi_1(s)$. This result will be used below.

Finally, the horizontal ocean current, projected in the plane (x,z), is given by the vector

$$V_c(z) = V_c\chi_c(z(s))i, \tag{2.2b}$$

where V_c is the current intensity at the sea level and $\chi_c(z(s))$ is the current profile along the cable.

2.1. Static parameters

Obviously, the dynamic response depends on the cable's static configuration and, in the context of the proposed asymptotic approximation, all static information can be synthesized in some few integral parameters to be introduced next. The first two of them are defined by

$$I_n = \frac{1}{l}\int_0^l |\chi_1(s)|^n \mathrm{d}s; \qquad n = 2, 3. \tag{2.3a}$$

It is not difficult to explain the physical origin of these integrals. In fact, since the lateral dynamic displacement is proportional to the static curvature ($v(s) \propto \chi_1(s)$), then the inertia force, integrated along the suspended length, should be proportional to I_2 in order to preserve the cable's lateral kinetic energy; for the same reason, the integrated viscous damping should be proportional to I_3 in order to preserve the dissipated power in the lateral motion.

However, in the presence of a strong horizontal ocean current $V_c\chi_c(z(s))$ the dynamic viscous force is, in first approximation, proportional to $V_c\chi_c(z(s)) \times \sin\theta(s) \times v(s)$ and then the dissipated power should be proportional to the integral I_c, where

$$I_c = \frac{1}{l}\int_0^l |\chi_c(z(s))\,\sin\theta(s)|\,\chi_1^2(s)\,\mathrm{d}s. \tag{2.3b}$$

It remains to define a parameter related to the restoring forces. As mentioned in the Introduction, there are two mechanisms for the cable to react to any imposed displacement: the first, by stretching the cable; the second, by adjusting the geometric configuration of the catenary. The ratio between these two restoring forces is known to be crucial in the cable dynamics and it is proportional to the coefficient Λ^2 where (see Ref. [6])

$$\Lambda = \frac{ql}{T_S} I_2^{1/2} \left(\frac{\mathrm{EA}}{T_S}\right)^{1/2} \left(\frac{l}{l+l'}\right)^{1/2}. \tag{2.3c}$$

For a *loose cable*, where the tangent at the suspended end is almost vertical ($\theta(l) \approx \pi/2$), one has $ql \cong T_S$ and, since $\mathrm{EA}/T_S \gg 1$, then $\Lambda \gg 1$ in this situation; typically $\Lambda \approx 50$ for a *loose cable*. For a *tight cable*, where the angle with the horizontal is small at the sea level ($\theta(l) \ll \pi/2$), vertical equilibrium implies in $ql/T_S = \sin\theta(l) \ll 1$ and then $\Lambda \approx 5$.

Those are the only parameters that depend directly on the static configuration of the cable, the remaining ones, to be defined next, depending on the dynamic properties of the cable and on the imposed excitation.

2.2. Dynamic parameters

For a *heterogeneous* cable, as a mooring line usually is, the weight $q(s)$, mass $m(s)$, added mass $m_a(s)$, diameter $D(s)$, stiffness $\mathrm{EA}(s)$ and drag coefficient $C_D(s)$ change along the suspended length. Enforcing conservation of kinetic energy, and recalling that $v(s) \propto \chi_1(s)$, the averaged mass and added mass for the dynamic problem can be defined by the expressions

$$\{m; m_a\} = \frac{1}{I_2}\frac{1}{l}\int_0^l \{m(s); m_a(s)\}\chi_1^2(s)\,\mathrm{d}s,$$

$$D = \sqrt{\frac{4m_a}{\rho\pi}}; \qquad q = \frac{1}{l}\int_0^l q(s)\,\mathrm{d}s; \tag{2.4a}$$

$$\frac{1}{\mathrm{EA}} = \frac{1}{l}\int_0^l \frac{\mathrm{d}s}{\mathrm{EA}(s)},$$

with D being the *equivalent* diameter and $\{q;\mathrm{EA}\}$ the averaged weight and stiffness. In a similar way, enforcing conservation of the dissipated power, the averaged drag coefficients are defined by

$$C_{D,0} = \frac{1}{I_3}\frac{1}{l}\int_0^l C_D(s)\frac{D(s)}{D}|\chi_1(s)|^3\mathrm{d}s,$$

$$C_{D,c} = \frac{1}{I_c}\frac{1}{l}\int_0^l C_D(s)\frac{D(s)}{D}|\chi_c(z(s))\,\sin\theta(s)|\chi_1^2(s)\,\mathrm{d}s, \tag{2.4b}$$

where $C_{D,0}$ is to be used in the absence of an ocean current and $C_{D,c}$ when the ocean current is strong; a more

appropriated definition for the drag force in an intermediate situation is introduced in Section 4. The related damping coefficients are given by the expressions

$$\zeta_0 = \frac{8}{3\pi}\frac{2C_{D,0}}{\pi}\frac{\rho\pi D^2/4}{m+m_a}\frac{T_S}{ql}\frac{I_3}{I_2^2}\frac{\sigma_U}{D},$$
$$\zeta_c = \frac{2C_{D,c}}{\pi}\frac{\rho\pi D^2/4}{m+m_a}\frac{2V_c}{\omega D}\frac{I_c}{I_2}, \tag{2.5}$$

with ω being the frequency of the imposed displacement and σ_U its rms value, see Eq. (2.7a).

As discussed in the Introduction, there are two time scales related to the distinct mechanisms for the restoring forces; the associated frequencies are

$$\omega_c = \frac{\pi}{l}\sqrt{\frac{T_S}{m+m_a}}, \qquad \omega_e = \frac{\pi}{l+l'}\sqrt{\frac{EA}{m}}. \tag{2.6}$$

The frequency ω_c is the natural frequency of an horizontal cable with length l subjected to the traction T_S and with mass $m + m_a$; the frequency ω_e is the elastic axial frequency of a cable with length $l + l'$, axial stiffness EA and mass m. Obviously, they are not the actual natural frequencies of the cable, neither they intended to be: they serve only as reference values. In this context, in particular, it can be checked that $\omega_c/\omega_e \approx (T_S/EA)^{1/2} \ll 1$, as anticipated in the Introduction.

From some simple considerations it is not difficult to estimate the order of magnitude of ω_c. In fact, from the equilibrium of a catenary one has $T_S = ql/\sin\theta(l)$ and, since $q = (m - m_a)g$ for an homogeneous cable, then $\omega_c \approx \pi(g/h)^{1/2}$, where the water depth h is assumed of order of the suspended length l. It turns out that $P_c = 2\pi/\omega_c \approx 2(h/g)^{1/2} \approx 20$ s. for a water depth $h \approx 1000$ m and the wave frequency ω is of order of magnitude of ω_c, implying in $\omega/\omega_e \ll 1$. This is the essential assumption in the derived asymptotic approximation for the dynamic tension, as discussed in the Introduction and further elaborated in the Section 4. Also, notice that the dynamic excitation is important only in deep water: in shallow water ($h \approx 10$ m) one has, in general, $\omega \ll \omega_c$ and the cable response is quasi-static.

2.3. Excitation parameters

The dynamic motion of the cable is excited by the displacement $U(t) = U_0\cos(\omega t)$ imposed at the suspended end S in the *tangent* direction. Instead of using the displacement amplitude U_0 the following parameters will be introduced here

$$\sigma_U = \langle U^2(t)\rangle^{1/2} = U_0/\sqrt{2}, \qquad a = \frac{U_0}{\sigma_U}, \tag{2.7a}$$

where σ_U is the rms of the imposed displacement and a is the normalized 'wave envelop'. The reason for this is solely editorial: Eq. (2.7a) can be extended directly to a random excitation, to be addressed in an accompanying paper. The *elastic tension* T_e is defined accordingly by

$$T_e = EA\frac{\sigma_U}{l+l'}, \tag{2.7b}$$

while the information about the imposed wave frequency ω can be introduced through the non-dimensional parameter

$$\Omega = \frac{\pi}{\Lambda}\left(\frac{\omega}{\omega_c}\right). \tag{2.7c}$$

Notice that for the same value of ω/ω_c the *reduced frequency* Ω is larger for a tight cable, where Λ is smaller. As expected, this means that the 'freezing situation', where the imposed displacement is absorbed elastically, is more likely to occur in a tight cable than in a loose one.

2.4. The algebraic expression for the dynamic tension

As discussed in the Introduction, the dynamic tension is essentially constant along the cable when $\omega/\omega_e \ll 1$. Under this same condition it is also possible to show that the lateral dynamic displacement is, in first approximation, proportional to the static curvature, or $v(s) \cong V\chi_1(s)$, where V is the displacement amplitude and $\chi_1(s)$ is defined in Eq. (2.2a). Within this approximation, it follows that the relevant dynamic variables are reduced to two discrete values, the amplitudes of the dynamic tension and of the lateral displacement. Integrating the equilibrium equations in the transversal and axial directions, together with the equation for the geometric compatibility, one obtains, with the help of the integral parameters introduced in Section 2.1, two algebraic equations with these two unknowns. Solving this system the dynamic tension can be determined. The mathematical derivation is elaborated in Section 4, the final result being given below. In this way, if the dynamic tension is written in the form

$$\hat{T}_D(s,t) = T_D(s)\,e^{-i\omega t},$$
$$\tau_D(s) = \frac{T_D(s)}{T_e} = \tau(s)\,e^{i\phi(\omega;s)}, \tag{2.8a}$$

it can be shown that the non-dimensional dynamic tension amplitude $\tau(s)$ is given by

$$\tau(s) = \left[\frac{c_1(s)\left(\sqrt{b^2(\Omega) + (4\zeta_0^2/\Omega^4)a^2} - b(\Omega)\right)^2 + 2c_2(s)\left(\sqrt{b^2(\Omega) + (4\zeta_0^2/\Omega^4)a^2} - b(\Omega)\right)}{(4\zeta_0^2/\Omega^4)}\right]^{1/2} \tag{2.8b}$$

with

$$b(\Omega) = \left(\frac{1-\Omega^2}{\Omega^2}\right)^2 + \zeta_c^2,$$

$$c_1(s) = \left(1 - \frac{l}{l+l'}\pi^2\left(\frac{\omega}{\omega_e}\right)^2\frac{s}{l}\right)^2,$$

$$c_2(s) = \left[1 + \frac{1-\Omega^2}{\Omega^2}\frac{l}{l+l'}\pi^2\left(\frac{\omega}{\omega_e}\right)^2\frac{s}{l}\right]^2 + \zeta_c^2 c_1(s). \tag{2.8c}$$

Notice that Eqs. (2.8a)–(2.8c) already incorporates the variation of the dynamic tension along the suspended length. In general this variation is weak, since the term in s/l is multiplied by the small parameter $(\omega/\omega_e)^2$, but in certain circumstances, when $\Omega \ll 1$, it may become important, as discussed below.

It seems worthwhile at this point to analyze Eqs. (2.8a)–(2.8c) in some limit situations, where then the obtained result can be more easily interpreted. In this way, consider Eq. (2.8a) when $\Omega \gg 1$ (but keeping $\omega/\omega_e \ll 1$). With an error of the form $[1 + O((\omega/\omega_e)^2; 1/\Omega^2)]$ one has $\{c_1(s) = 1;\ b(\Omega) = c_2(s) = 1 + \zeta_c^2\}$ and so, from Eq. (2.8b), it follows that $\tau(s) = a$. Also, when $\sigma_U/D \gg 1$ one has $\zeta_0 \gg 1$, see Eq. (2.5), and then from Eq. (2.8b) it follows, with an error of the form $[1 + O((\omega/\omega_e)^2; D/\sigma_U)]$, that again $\tau(s) = a$. In both cases one obtains (see Eqs. (2.7a) and (2.7b))

$$|T_D(s)| \to \mathrm{EA}\frac{U_0}{l+l'}, \qquad (\omega/\omega_c; U_0/D) \gg 1, \tag{2.9a}$$

that is exactly the result anticipated at the Introduction: the *elastic limit* can be reached when either the imposed amplitude or the wave frequency becomes large.

In the other limit, when $\Omega \ll 1$, one has $b(\Omega) = 1/\Omega^4 \gg 1$ and from Eq. (2.8b) it follows, with an error of the form $[1 + O(\Omega^4)]$, that

$$\tau(s) = \left(c_1(s)\zeta_0^2 a^2 + c_2(s)\right)^{1/2} a\Omega^2,$$

$$c_2(s) = \left[1 + \left(\Lambda\frac{\omega_c}{\omega_e}\right)^2\frac{s}{l}\right]^2 + \zeta_c^2 c_1(s). \qquad (\Omega \ll 1) \tag{2.9b}$$

There are two situations where Ω can become small: one, when the imposed frequency is effectively low and $\omega/\omega_c \ll 1$; the other, when the cable is *loose* ($\Lambda \gg 1$) and Ω can be small even when $\omega/\omega_c \cong O(1)$. The first case is of little importance in deep water and, furthermore, this limit is not well described by Eq. (2.9b): when $\omega/\omega_c \ll 1$ one should use a quasi-static solution, as described in Ref. [2] and discussed in Section 4. However, if Λ is so large that $\Lambda(\omega_c/\omega_e) \cong O(1)$, as it may happen in a *loose cable*, the dynamic tension is in fact small when compared with the elastic tension T_e, since $\tau \cong O(\Omega^2) \ll 1$, but the variation of $\tau(s)$ along the suspended length cannot be disregarded, once $dc_2/ds \cong O(1)$. Furthermore, although small when compared to T_e, the dynamic tension may be comparable to the static tension and should not be ignored.

The algebraic expression (2.8a)–(2.8c), albeit simple, recovers qualitatively the main features of the dynamic tension in a submerged cable. If it is also shown that it is quantitatively consistent, then it provides an interesting simplification for the proposed problem, with possible imbrications in others directions too. The quantitative aspect will be addressed next, the possible imbrications being reserved to the accompanying papers.

3. Experimental and numerical verification of Eqs. (2.8a)–(2.8c)

In this section the algebraic approximation (2.8a)–(2.8c) for the amplitude of the dynamic tension is compared with some experiments and with numerical results obtained from two distinct time domain programs. Only a survey of this rather extensive set of comparisons will be presented here, the intention being to show the typical adherence among these results and to draw attention, in certain particular cases, to some observed disagreements, commentating them in the light of the perturbations introduced on the continuous models by the discretization.

3.1. Experimental results

In a research project sponsored by Petrobras, Ref. [1] analyzed at the USP wavetank the dynamic behavior of mooring lines; in the experiments, a chain, anchored in a point on the wavetank floor, was excited dynamically at the suspended end. The imposed motion was harmonic, the displacement being either along a straight line or else circular, and the measured output was *the total tension at the suspended end*. Two different chains, with relatively discrepant properties, were tested in several geometric configurations and the dynamic excitation varied too, in amplitude, frequency and type of motion (if straight or circular). Around a hundred different tests were made and, obviously, only a small sample of them will be discussed here. However, the results to be presented are typical, being representative of all experiments realized.

The relevant physical properties of the two chains are given in Table 1 and the *static configuration* can be characterized by the geometric parameters (h; θ_s; l_T), where h is the water depth, $\theta_s = \theta(l)$ is the angle at the suspended end and l_T the total chain length; since the friction on the wavetank floor can be ignored, $l' = l_T - l$.

Table 1
Physical properties of the two chains (Ref. [1])

Chain	EA (N)	q (N/m)	D (m)	m (kg/m)	m_a (kg/m)	C_D
1	4763	0.360	0.0026	0.042	0.013	1.6
2	17664	0.865	0.0041	0.088	0.027	1.6

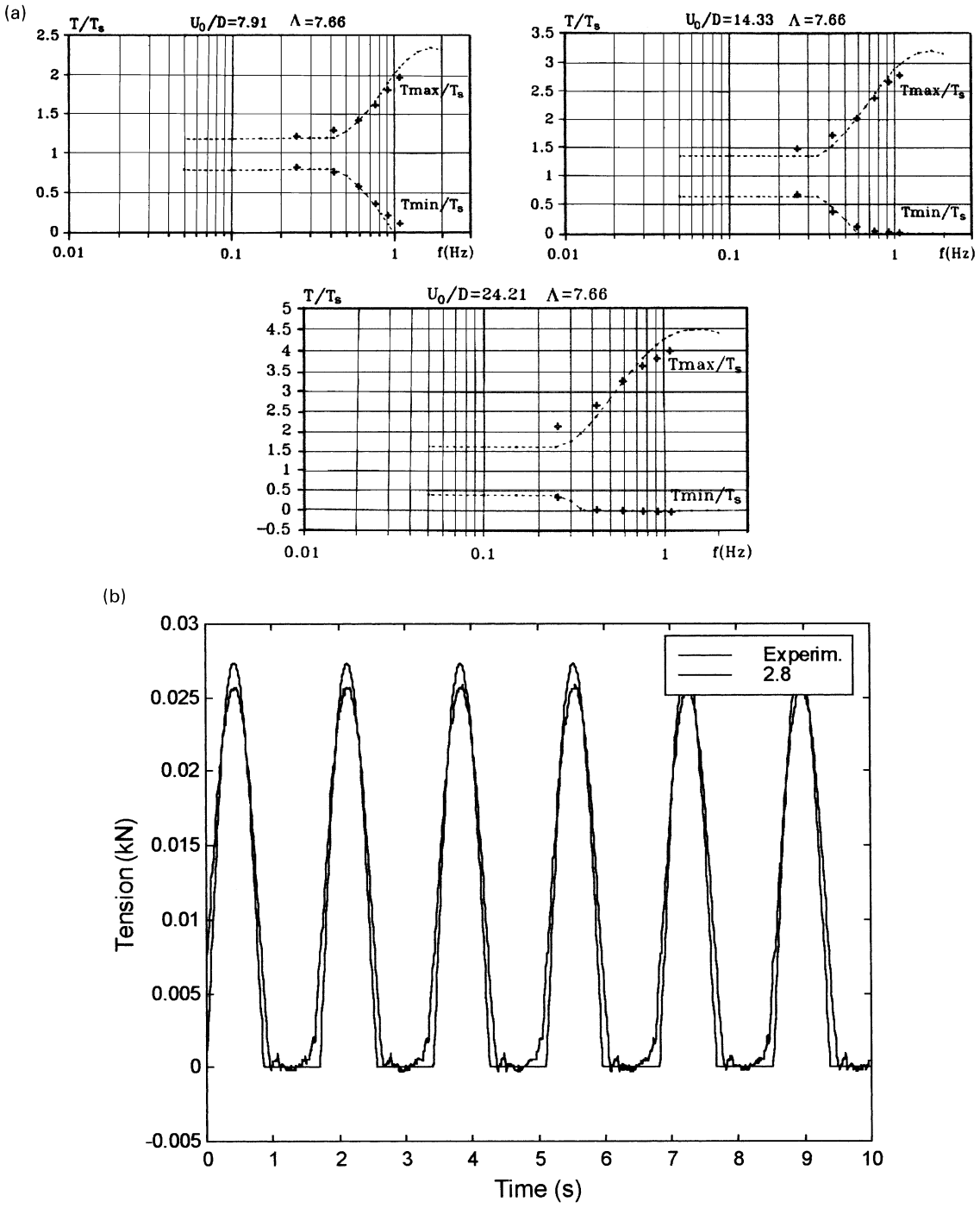

Fig. 1. (a) Total tension at the *suspended end*. Experiments (+); Eqs. (2.8a)–(2.8c) (- - -). (a) $U_0/D = 7.91$; (b) $U_0/D = 14.33$; (c) $U_0/D = 24.21$. Chain 2, $\Lambda = 7.66$. (Source: Ref. [1]). (b) Variation of tension in time: experiment (—); Eqs. (2.8a)–(2.8c) (- - -) $U_0 = 0.076$ m; $f = 0.658$. Chain 1, ($h = 1.82$ m; $\theta_S = 13.8°$; $l_T = 28.73$ m), $\Lambda = 2.6$.

The first set of results, presented in Fig. 1a, shows the plot of the maximum and minimum values of the total tension in a cycle as a function of the imposed frequency f (Hz). The tension has been normalized by the static value T_s, see Eq. (2.1a), and the theoretical values have been determined by the expression $T_{\max;\,\min} = 1 \pm \tau(l)(T_e/T_S)$, with $\tau(l)$ given by Eqs. (2.8a)–(2.8c) and T_e by Eq. (2.7b); obviously, when $T_{\min}$ resulted negative in this expression then the value $T_{\min} = 0$ was taken, since the chain cannot support any compression. In all tests of Fig. 1a chain 2 was used in the static configuration given by ($h = 2.02$ m; $\theta_S = 11.2°$; $l_T = 20.3$ m), and only the amplitude U_0 of the imposed circular motion was changed, as defined in the figure caption. The agreement between the experimental and

theoretical values is quite good, even more if it is observed that in several cases, identified by the result $T_{min} = 0$ at the suspended end, the chain slackens as a whole. This is really a demanding test for the algebraic approximation: in fact, the larger influence of the geometric nonlinearity is expected to happen for a *tight* cable (small θ_S) under strong dynamic excitation, as in the cases tested, but the algebraic approximation does not include this nonlinearity, the only nonlinear term in Eqs. (2.8a)–(2.8c) being the viscous dissipation, see Section 4. The observed concordance shows that the geometric nonlinearity is, indeed, of little concern for this class of problems. The only point that deserves a further comment is the following: as explained in Section 4, Eqs. (2.8a)–(2.8c) ceases to be valid in very low frequency, where a quasi-static solution must be used; the two horizontal lines in Fig. 1a represent just this solution. This low frequency correction has not been incorporated in the final solution because it has little importance in deep water.

In order to display the generality of the experimental results and, at the same time, to point out some more subtle aspects of the problem, Fig. 1b shows, for a different chain in a distinct geometric configuration, the variation in time of the total tension at the suspended end. Again, a close agreement is observed, indicating now that the cable's response is in fact 'harmonic', the experimental result not showing evidences of higher harmonics.

This same problem was solved by a time domain numerical program, see Fig. 2a. The overall response is comparable to the experiment, although two peculiarities are conspicuous and should be commented: first, it is now clear the evidences of higher harmonics; second, the tension becomes negative in a short time interval, in spite of the fact that the chain cannot support a compressive force. Both phenomenons cannot be real, since they do not appear in the experiments, and so they must be due to the discretization. A possible explanation for the observed higher harmonics is the *impact forces* on the 'lumped' masses when they hit the ground: they give rise then to high frequency oscillations that are propagated through the cable with a small dissipation, unless the axial damping is assumed to be very large. This may be indeed one of the resons why numerical codes sometimes encounter difficulties to converge when the sea floor is rigid, the numerical integration becoming easier when the ground is assumed 'soft'. These higher harmonics, although spurious in the continuum problem, are innate in the discrete system and so, once generated; they interact with each other blurring the tension signal. As an example, Fig. 2b shows, for a random excitation, the time history of the touchdown tension of a riser with EJ = 0.

Notice not only the large magnitude of the (unduly) compression but also how the higher frequency components apparently enhance the value of the maximum tension.

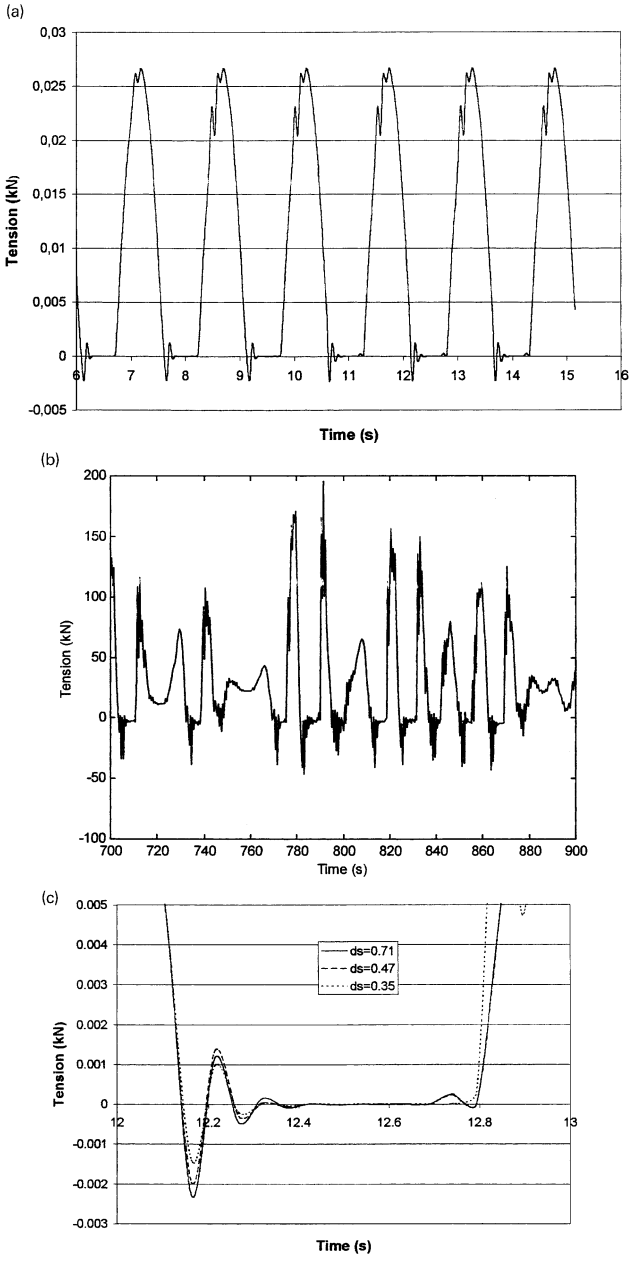

Fig. 2. (a) Same as Fig. 1b but obtained from a time domain program (Orcaflex). (b) Tension at the touchdown of an actual riser in random excitation. EJ = 0. (c) Compressive force as a function of the mesh size ds (same problem of (b)).

Furthermore, if EJ ≠ 0, as it is usually, some compression is acceptable, although it is not known a priori how much. This is the main motivation of the accompanying paper on dynamic compression.

Table 2
Parameters of the risers simulated by Orcaflex and Cable (friction coefficient: $\mu = 0.4$; axial damping: $\zeta_{AXIAL} = 10\%$)

	D (m)	m (kg/m)	EA (kN)	EJ (kN m^2)	C_D
(FR)	0.2160	67	1.92×10^5	9.84	1.0
(SR)	0.2191	70	2.10×10^6	9241	1.1

Table 3
Parameters of the heterogeneous mooring line: Chain 1–Cable–Chain 2 (friction coefficient: $\mu = 0.4$; axial damping: $\zeta_{AXIAL} = 10\%$)

	m (kg/m)	m_a (Kg/m)	q (kN/m)	EA (kN)	D (m)	C_D	l_c (m)
Chain 1	203	27.58	1.920	7.94×10^5	0.095	2	3800
Cable	49	9.56	0.387	5.37×10^5	0.109	2	1000
Chain 2	160	21.56	1.513	6.27×10^5	0.084	2	200

Table 4
Current profile on the simulations ($z^* = h - z$; $h = 1000$ m)

z^* (m)	0	50	100	140	230	340	415	545	640	785	1000
V (m/s)	1.70	1.54	1.39	1.18	0.72	0.78	0.01	−0.28	−0.36	−0.53	0.00

It is certainly expected that this numerical ill behavior should disappear as the mesh size becomes thinner. As an example, Fig. 2c retakes the problem of Fig. 2a, showing that indeed the compressive force tends slowly to zero as the mesh size diminishes. On the other hand, and this is shown clearly in Fig. 2b, it is not uncommon to use, in a real problem, a reasonably small mesh size and, in spite of this, to obtain a response where high frequency oscillations and a compression force above the 'critical value'[2] appear in a somewhat strong way, making difficult to assess the correct behavior of the cable's dynamic. It can be argued that these differences are of little concern in a real design of a cable, and one should agree with this observation in most cases; however, they may become important when the numerical solution is used as paradigm to verify the quality of the analytical approximation, and this is the point of concern here. More is going to be said about this question in the Section 3.2.

3.2. Numerical results

Two cables, one representing a *flexible riser* (FR) and the other a *steel riser* (SR), with typical parameters defined in Table 2, were numerically simulated under distinct environmental conditions using two different time domain programs, Orcaflex and Cable respectively. In this section, the obtained numerical results are compared with the algebraic approximation (2.8a)–(2.8c) in order to check not only its validity but also to display some particular features that deserve comments.

A *heterogeneous mooring line*, with properties defined in Table 3, see Eqs. (2.4a) and (2.4b), was also numerically simulated and the result is here compared to Eqs. (2.8a)–(2.8c). To complete the verification of the theoretical result it would be necessary to check the behavior of a cable with concentrated forces, due to either a buoy or a weight, but this case has not been addressed in the numerical analysis. A simple catenary configuration was assumed in all simulations.

The friction coefficient between the sea floor and the cable and the axial damping factor were always the same, respectively $\mu = 0.4$ and $\zeta_{AXIAL} = 10\%$; also the cable's total length was so large that the *effective length* was almost always[3] given by $l' = T_0/\mu q$. The imposed motion at the suspended end was circular, harmonic, with amplitude A and period $P = 2\pi/\omega$, and the static configuration was identified by the angle θ_S at the suspended end. The horizontal ocean current, when present, had a depth profile defined in Table 4, typical of Campos Basin.

3.2.1. Numerical results: flexible riser ($h = 1000$ m)

Fig. 3a and b present, for the flexible riser, the dynamic tension T_D at the touchdown as a function of the angle θ_S of the static configuration. The wave period was kept constant, given by $P = 11.5$ s, and two distinct amplitudes for the circular motion were assumed: $A = 2.77$ and 5.54 m. The water depth was 1000 m and the dynamic tension T_D was normalized by the tension $(T_0 + T_R)$, where T_0 is the static tension at the touchdown and $T_R = 10$ tons is a reference value given by the fabricant; obviously, the simple relation T_D/T_0 becomes unbounded when $\theta_S \to \pi/2$ and it was thus avoided. In Fig. 3b the angle θ_S is the one observed in the absence of a current; after the current is 'turned on' the static configuration is changed and the parameters (2.8a)–(2.8c) are then computed.

In both cases (w/o or w/ current) the agreement between Eqs. (2.8a)–(2.8c) and the numerical results from Orcaflex is fairly good for the smaller amplitude $A = 2.77$ m; for the larger amplitude the general trend is similar but the discrepancies are obviously more apparent. Fig. 4a helps to explain this fact: here the static configuration and the period were kept constant ($\theta_S = 80.5°$; $P = 11.5$ s) but the imposed amplitude was changed. For the smaller amplitudes the agreement among the numerical results themselves, obtained from Cable and Orcaflex programs,[4] are good, and so they are with Eqs. (2.8a)–(2.8c); however, as the amplitude increases the concordance with Eqs. (2.8a)–(2.8c) deteriorates, in general, but so it does among the numerical results. Furthermore, the algebraic approximation

[2] An analytical expression for this *critical load* P_{cr} is derived in the second paper of this series. Obviously, for the chain one has that $P_{cr} = 0$.

[3] When this condition is not fulfilled the total length l_T is given in the figure caption.

[4] Details about the Cable program can be found in Ref. [5] and some discussion about the Orcaflex program in Ref. [7].

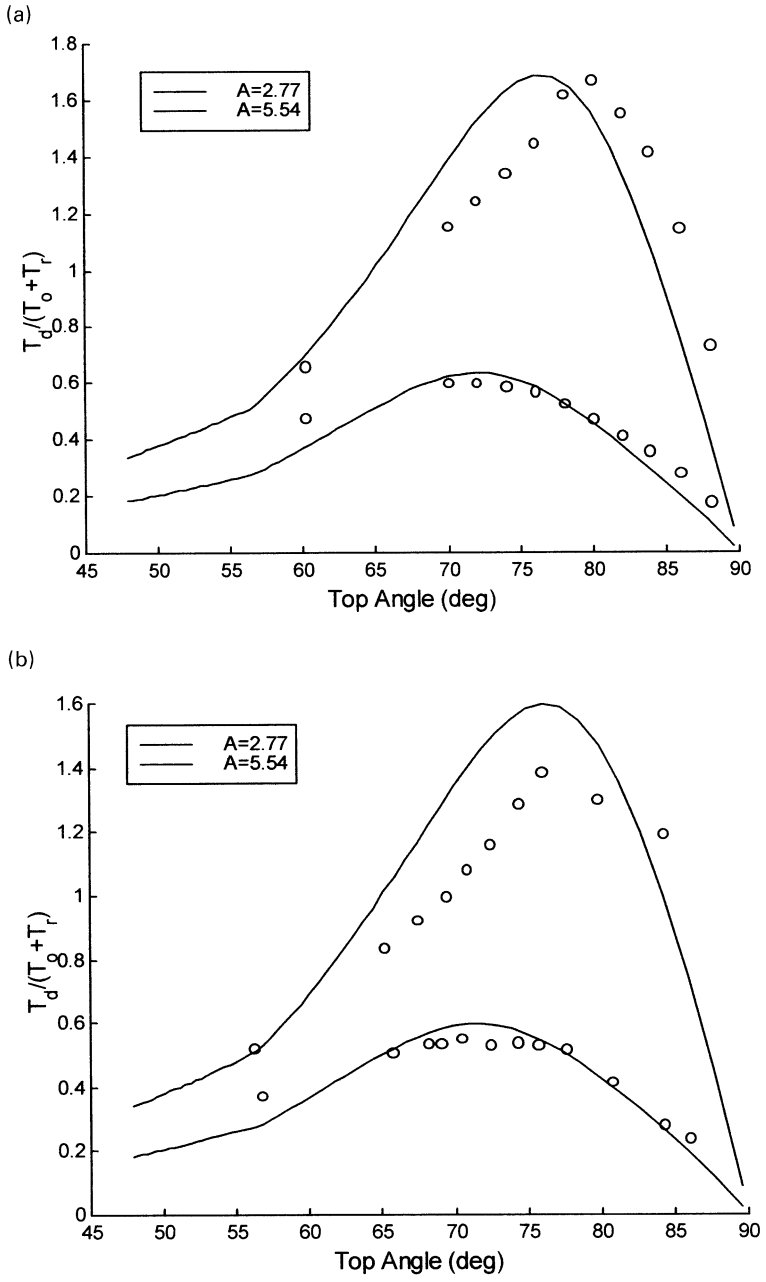

Fig. 3. (a) Dynamic tension at the *touchdown* (FR) as a function of θ_S. (w/o current; $P = 11.5$ s). (—) Eqs. (2.8a)–(2.8c); Orcaflex (○). (b) Dynamic tension at the *touch down* (FR) as a function of θ_S. (w/current; $P = 11.5$ s). (—) Eqs. (2.8a)–(2.8c); Orcaflex (○).

predicts a response somewhere in between the two numerical results. The impact forces on the discrete masses are possibly the reason for the observed deterioration when the amplitude increases: in this case, they generate at the touchdown high frequencies oscillations that are propagated along the cable with a relatively small damping,[5] and so they are weakly attenuated. To check this assumption, the highest point in Fig. 3a, corresponding to ($A = 5.54$ m; $\theta_S = 80.5°$; $P = 11.5$ s), was simulated again using now an axial damping three times larger. The obtained result, also shown in Fig. 4a, indicates that with this higher damping the concordance between Orcaflex and Eqs. (2.8a)–(2.8c) is much better. Notice that in the Cable program the foundation was assumed to be soft while in Orcaflex it was assumed to be rigid and, also, that the discrepancies increase just when $T_D/T_0 > 1$, namely, when the cable becomes dynamically compressed.

In the other hand, one should expect that the influence of these higher harmonics diminishes when both the static and dynamic tensions become large and the riser is not

[5] For a *Rayleigh damping* of the form $d\partial v/\partial t$, the damping factor becomes indeed very small in high frequency even when $\zeta_{AXIAL} = 10\%$ for the basic mode.

compressed at the touchdown. Fig. 4b gives support to this conclusion, once it displays the dynamic tension at the touchdown point as a function of the amplitude for ($\theta_S = 37.8°$; $P = 11.5$ s): although the maximum amplitude is now twice the one imposed in the other case, the agreement is very good here, among the numerical results themselves and with Eqs. (2.8a)–(2.8c) too.

Fig. 5 presents the dynamic tension at the *suspended end* normalized by the static tension T_S as a function of the amplitude, keeping constant ($\theta_S = 70°$; $P = 12$ s). The agreement is again fair enough for the smaller amplitudes but it becomes evidently discrepant for the larger amplitudes. In this same figure a fourth curve was plotted, named 'Orcaflex filtered': it corresponds to the sum of the two first harmonics of the Orcaflex response. Although the Orcaflex result seems to be lost for the

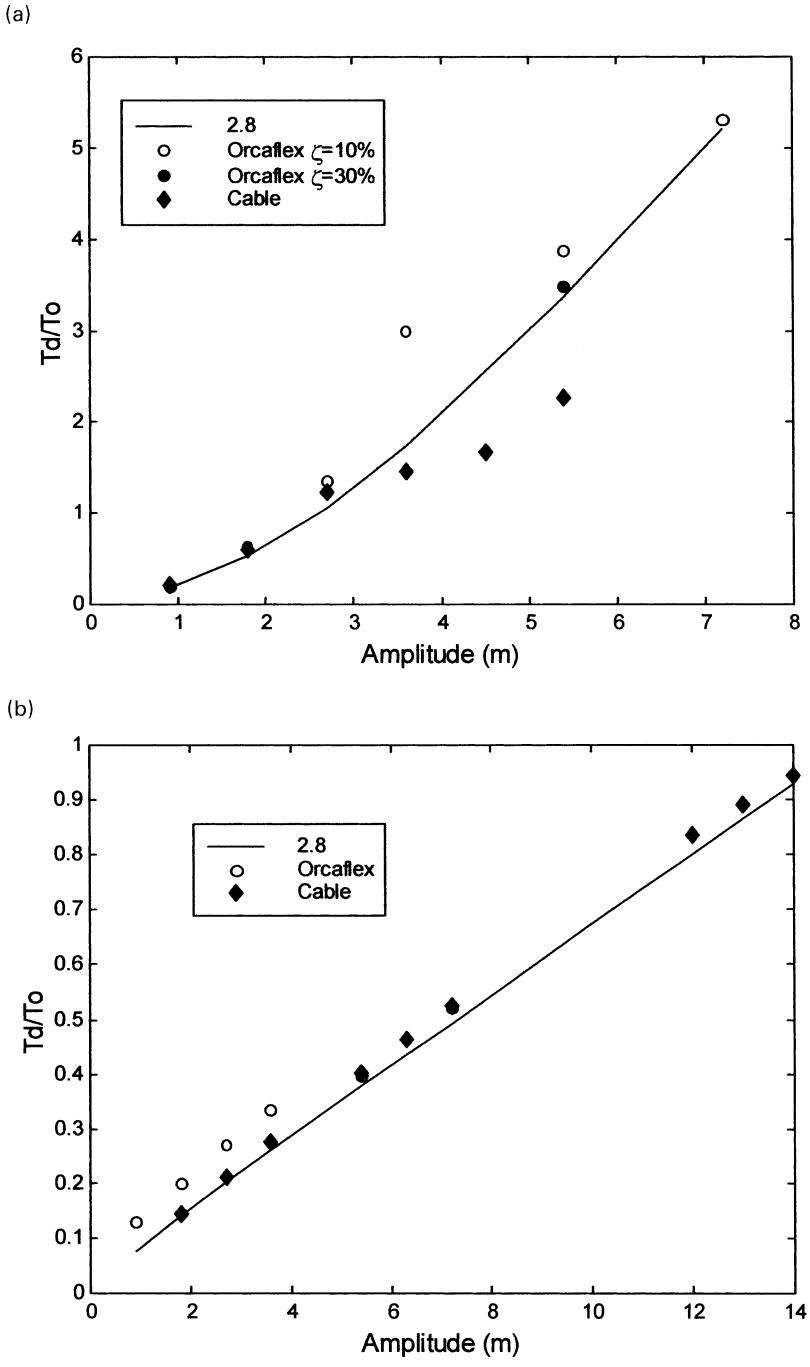

Fig. 4. (a) Dynamic tension at the *touchdown* (FR) as a function of amplitude ($\theta_S = 80.5°$; $P = 11.5$ s.; w/o current): (—) Eqs. (2.8a)–(2.8c); (○) Orcaflex; (◆) Cable; (●) Orcaflex with $\zeta_{AXIAL} = 30\%$. (Note: two first points of Cable and Orcaflex are coincident). (b) Dynamic tension at the *touchdown* (FR) as a function of amplitude ($\theta_S = 37.8°$; $P = 11.5$ s; w/o current); $l_T = 2800$): (—) Eqs. (2.8a)–(2.8c); (○) Orcaflex; (◆) Cable. (Note: last six points of Cable and Orcaflex are coincident).

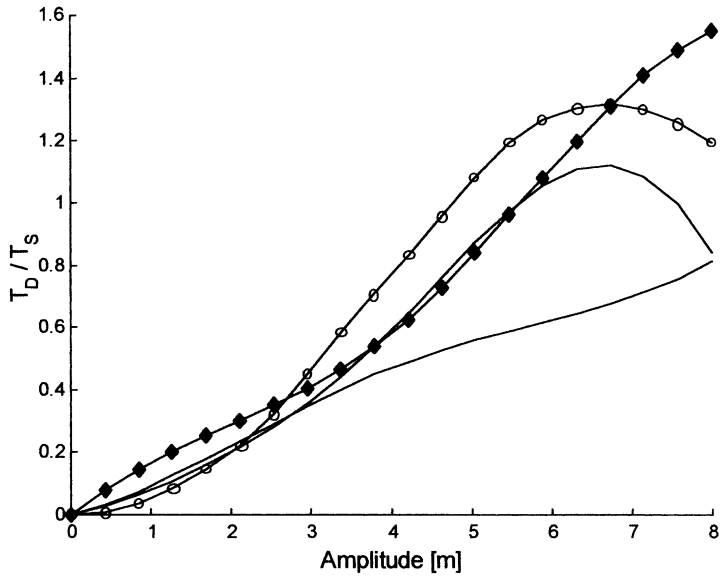

Fig. 5. Dynamic tension at the *suspended end* (FR) as a function of amplitude ($\theta_S = 70°$; $P = 12$ s; w/o current): (—) Eqs. (2.8a)–(2.8c); (-○-) Orcaflex; (-◆-) Cable; (- - -) Orcaflex Filtered.

highest amplitudes, since the dynamic tension decreases then when A increases, it should be noticed the close adherence between the filtered response and Eqs. (2.8a)–(2.8c), possibly indicating that the disagreement is due to the high frequency components.

This conjecture can be better visualized with a look to the corresponding time record in one period. Fig. 6a and b present, for $A = 2$ m, the total tension at the touchdown and at the suspended end normalized by the respective static tension as a function of the time. The agreement between the two numerical results and Eqs. (2.8a)–(2.8c) is quite good here, although it should be observed that it is less good at the suspended end: the Cable result is a little bit off and the Orcaflex time series shows evidences of a still incipient higher harmonics. This trend has been almost always observed, the agreement between the numerical results (and with Eqs. (2.8a)–(2.8c)) becoming worse, in general, at the suspended end. Fig. 6c and d repeat the same plots but for $A = 4$ m. Now Orcaflex results show the presence of strong high frequencies oscillations while Cable results, perhaps due to the soft foundation used, show a relatively smooth time series. However, the experimental results shown in Section 3.1 indicate that these high frequencies oscillations are in fact spurious, the influence of the soil stiffness being important only for the discrete systems (recall that in the experiments the fllor was rigid). Fig. 6c and d show, again, that the agreement is worse at the suspended end and that the 'filtered response' is closer to Eqs. (2.8a)–(2.8c).

3.2.2. Numerical results: steel riser ($h = 900$ m)

Fig. 7a and b show the plot of the dynamic tension at the *touchdown point* normalized by the static tension for a steel riser (SR). In Fig. 7a the static configuration is kept constant ($\theta_S = 80.5°$) and the tension is plotted as a function of the frequency for different amplitudes; in Fig. 7b the period is kept constant ($P = 8$ s) and the tension is plotted as a function of θ_S for different amplitudes. The agreement is fairly good in general, the error having a tendency to be magnified for the larger θ_S (smaller T_0) in Fig. 7b.

Fig. 8 shows the plot of the dynamic tension at the *suspended end* normalized by the static tension T_S as a function of the amplitude A; in all cases ($\theta_S = 70°$; $P = 12$ s). The agreement between the two numerical results and Eqs. (2.8a)–(2.8c) is again good for the smaller amplitudes but they become widely discrepant for the larger amplitudes, mainly the Cable result. The concordance between Orcaflex and Eqs. (2.8a)–(2.8c) is fair, although the Orcaflex result shows a tendency to an inflexion point, similar to the one observed in Fig. 5. Again, the behavior at the suspended end is worse than at the touchdown point but this is not restricted to expressions (2.8a)–(2.8c): as it is clear from the material presented here, the numerical results themselves become more discrepant at the suspended end for a reason not yet well understood. A possible explanation is the intense presence of high frequencies oscillations at this point, perhaps due to the small damping in the axial direction.

3.2.3. Numerical results: heterogeneous line ($h = 1000$ m)

The heterogeneous line defined in Table 3 was simulated by Orcaflex in the condition ($\theta_S = 58.5°$; $P = 10$ s) for different amplitudes of the tangent motion. Fig. 9 shows the comparison with Eqs. (2.8a)–(2.8c) of the obtained dynamic tension, normalized by the respective static tension, both at the suspended end (TOP) and at the touchdown point (TDP). The agreement is fair at the TDP, the

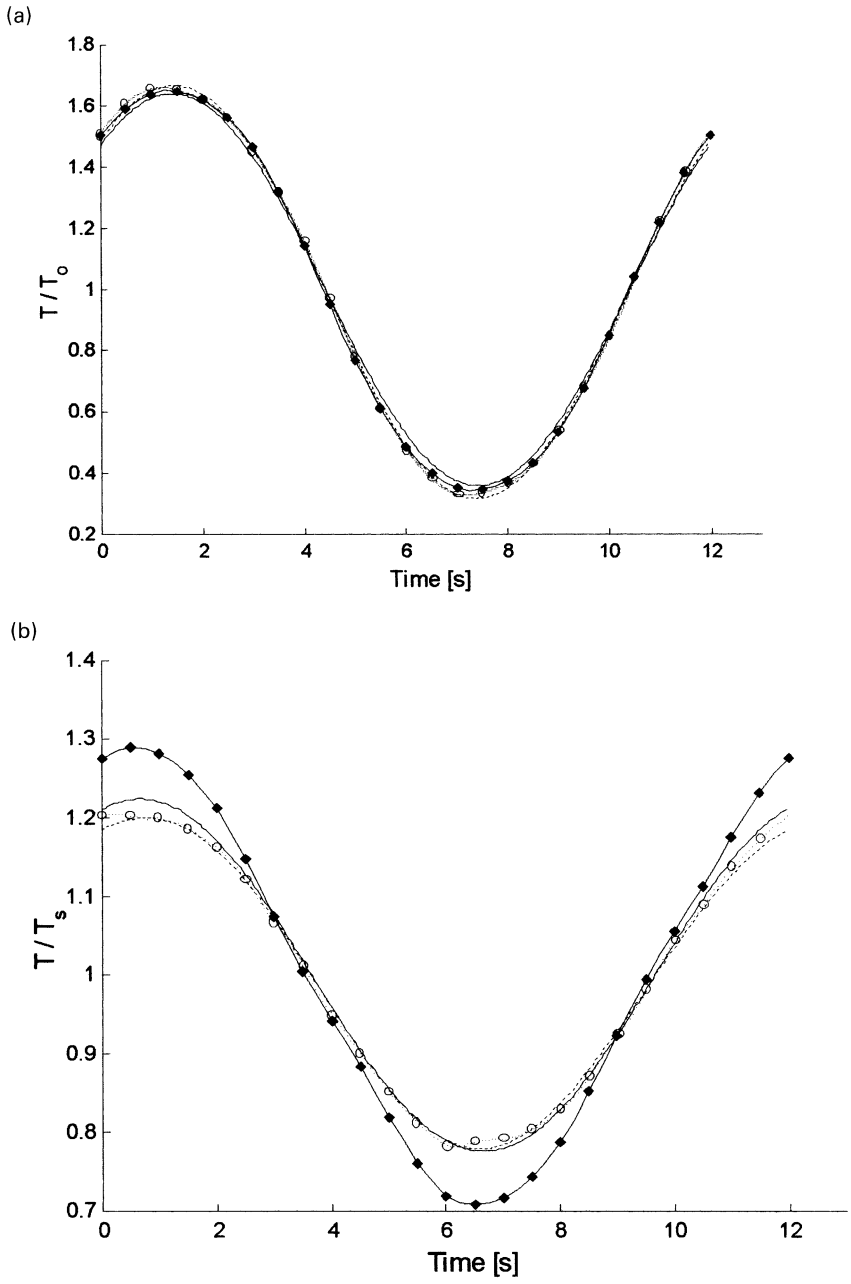

Fig. 6. (a) Total tension at the *touchdown* (FR) as function of time. ($A = 2$ m; $\theta_S = 70°$; $P = 12$ s; w/o current): (—) Eqs. (2.8a)–(2.8c); (-◆-) Cable; (-○-) Orcaflex; (- - -) Orcaflex Filtered. (b) Total tension at the *suspended end* (FR) as function of time. ($A = 2$ m; $\theta_S = 70°$; $P = 12$ s, w/o current): (—) Eqs. (2.8a)–(2.8c); (-◆-) Cable; (-○-) Orcaflex; (- - -) Orcaflex Filtered. (c) Total tension at the *touchdown* (FR) as a function of time. ($A = 4$ m; $\theta_S = 70°$; $P = 12$ s;w/o current): (—) Eqs. (2.8a)–(2.8c); (-◆-) Cable; (-○-) Orcaflex; (- - -) Orcaflex Filtered. (d) Total tension at the *suspended end* (FR) as function of time. ($A = 4$ m; $\theta_S = 70°$; $P = 12$ s; w/o current): (—) Eqs. (2.8a)–(2.8c); (-◆-) Cable; (-○-) Orcaflex; (- - -) Orcaflex Filtered.

difference increasing monotonically with the amplitude although the trend is not changed above the point where the line becomes dynamically compressed. At the TOP the agreement is not as good for the smaller amplitudes, the difference between Orcaflex and Eqs. (2.8a)–(2.8c) now decreasing monotonically with the amplitude.

3.3. Verification of Eqs. (2.8a)–(2.8c): conclusion

In this section, the algebraic expressions (2.8a)–(2.8c) has been compared with experimental and numerical results. The experiments, although restricted to tight configurations of mooring lines, show a very good adherence to Eqs. (2.8a)–(2.8c) in all cases (around a hundred) tested, even in extreme situations. At the same time they make evident a sort of numerical ill-behavior, also observed in other situations, related to the presence of high frequency oscillations and of a compression force in a cable with $EJ = 0$.

The numerical results, from two different programs and

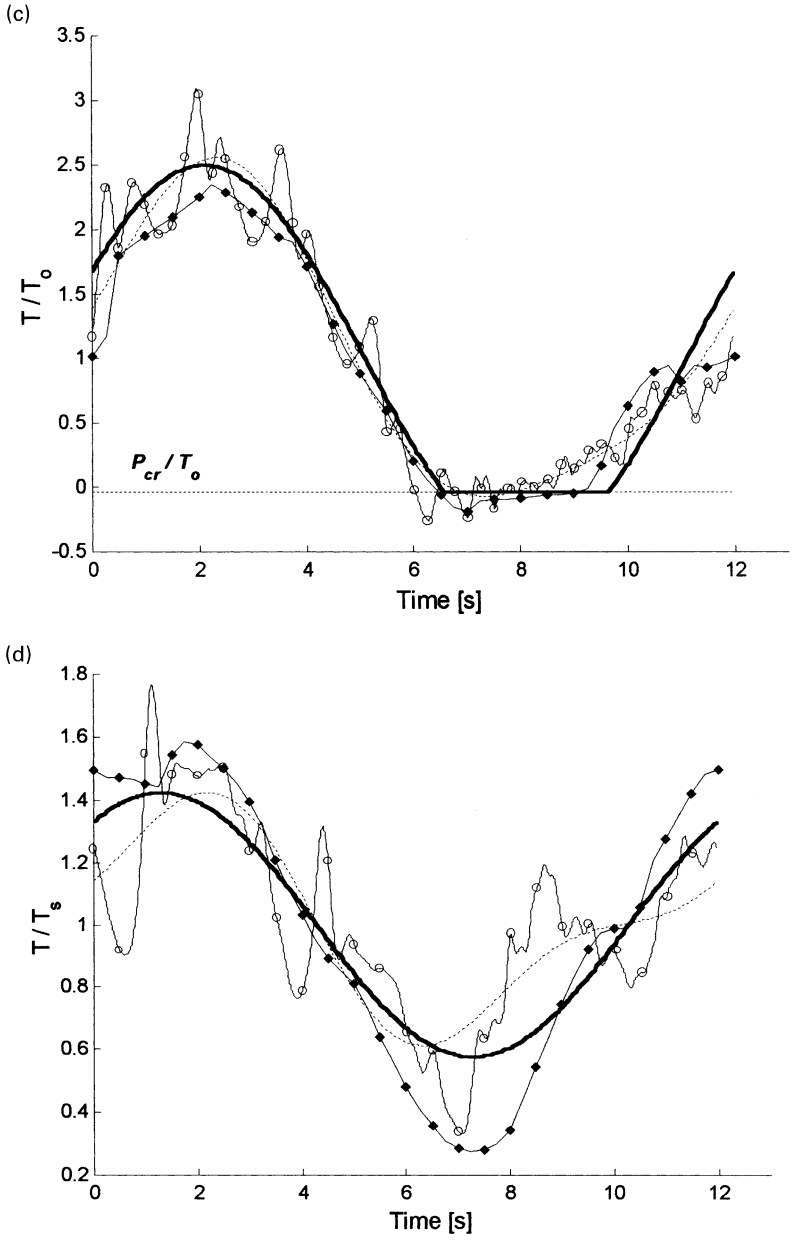

Fig. 6. (*continued*)

for three cables (flexible riser, steel riser and heterogeneous mooring line), in distinct static configurations and under a variety of dynamic excitation, show a general trend that can be summarized as follows: for a small to mild amplitude of the imposed motion, where the dynamic tension is of the order of the static tension at most, the numerical results agree among themselves as well with Eqs. (2.8a)–(2.8c); for the larger amplitudes, where then the dynamic tension becomes greater than the static tension, the numerical results diverge from Eqs. (2.8a)–(2.8c) and equally among themselves. Observing the close agreement between Eqs. (2.8a)–(2.8c) and the experiments even in an extreme condition, one would be tempted to rely more on Eqs. (2.8a)–(2.8c) than on the numerical solutions in these extreme situations, although a more comprehensive experimental program would certainly be welcomed to confirm this impression. The agreement at the suspended end is in general worse than at the touchdown point, a difficulty also observed when comparing the numericl results themselves. It is not clear why the numerical results show this tendency at this point, a possible explanation is suggested from the derivation of Eqs. (2.8a)–(2.8c): the variation of the dynamic tension along the suspended length is, as elaborated in Section 4, a 'second order' correction and it appears more strongly when the dynamic tensions are small. In this situation a larger relative discrepancy seems to be more likely expected even for the numerical solutions.

The spurious high frequency oscillations as well the

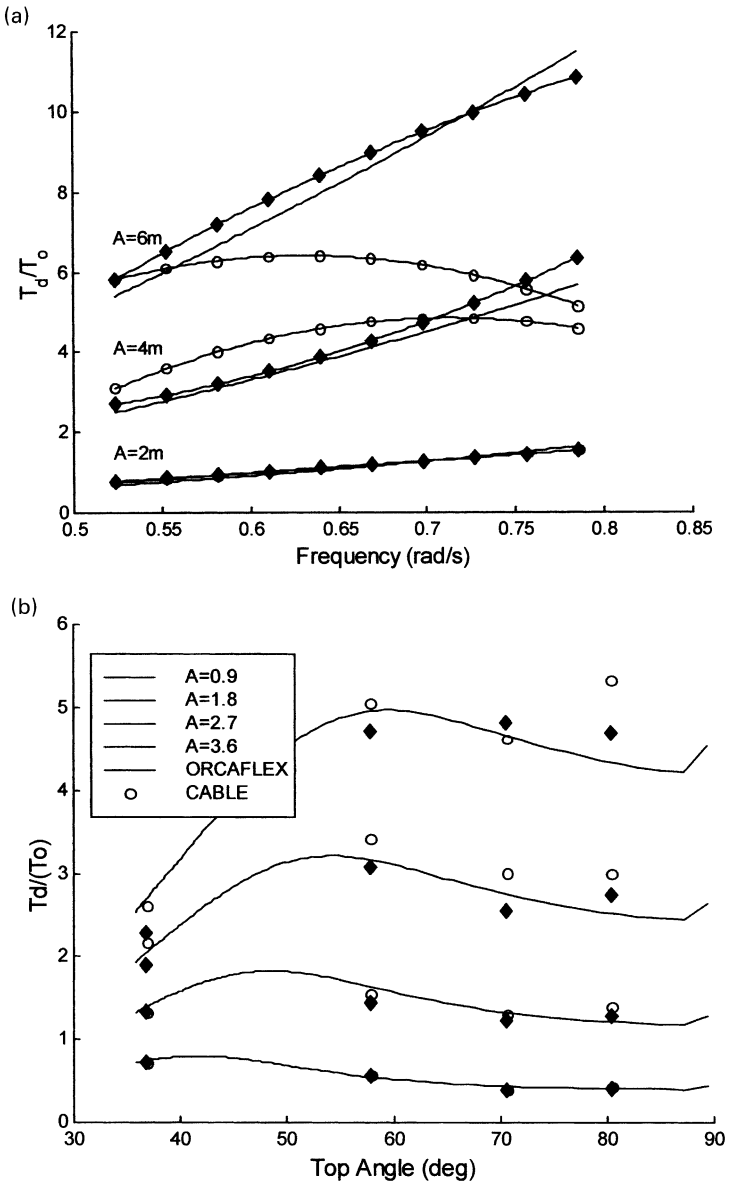

Fig. 7. (a) Dynamic tension at the *touchdown* (SR) as a function of frequency ($\theta_S = 70°$; w/o current): (—) Eqs. (2.8a)–(2.8c); (-◆-) Cable; (-o-) Orcaflex. (b) Dynamic tension at the *touchdown* (SR) as function of θ_S ($P = 8$ s; w/o current): (—) Eqs. (2.8a)–(2.8c); (○) Orcaflex; (◆) Cable (note: cable and Orcaflex are coincident at $A = 0.9$ m).

compression above the critical value, both caused by the discretization, tend to disappear as the mesh size diminishes. No effort was made in the present work to advance further in this direction, the focus being concentrated more to cover a wide range of situations rather than a specific case in depth. Only one example about the inflence of discretization was discussed here, see Fig. 2c.

On the other hand, the algebraic approximation (2.8a)–(2.8c) has to be looked with caution when the suspended length is so large that the assumption $\omega/\omega_e \ll 1$ is not satisfied. However, this situation is unlikely to occur in a real problem unless the material is intrinsically soft, as in the case of the 'synthetic cables' that are being used lately. The algebraic expression has to be revised in this case but this is beyond the scope of the present work.

4. Mathematical derivation of Eqs. (2.8a)–(2.8c)

As seen in the Introduction, the *static configuration* is defined by the functions $\{\theta(s); T(s)\}$, where $\theta(s)$ is the angle between the tangent to the cable and the horizontal plane and $T(s)$ is the static tension. The *dynamic variables* are given by

$$\{\hat{u}(s,t); \hat{v}(s,t); \hat{\varphi}(s,t); \hat{T}_D(s,t)\},$$

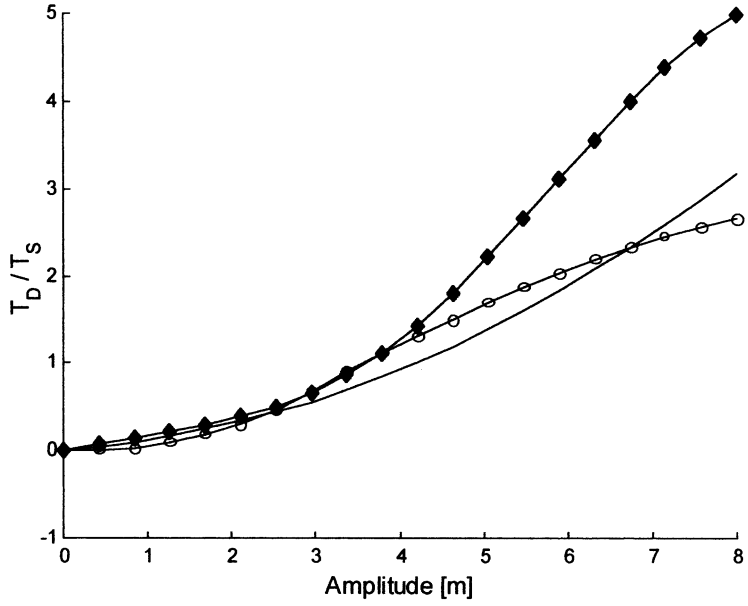

Fig. 8. Dynamic tension at the *suspended end* (SR) as function of amplitude ($\theta_S = 70°$; $P = 12$ s; w/o current): (—) Eqs. (2.8a)–(2.8c); (-○-) Orcaflex; (-◆-) Cable.

respectively, the axial displacement, the transversal displacement, the dynamic variation of the angle $\theta(s)$ and the dynamic tension. Assuming, as it seems reasonable, that the dynamic displacement is small compared to either the suspended length l or the static angle $\theta(s)$, the dynamic equations can be derived ignoring the geometric non linearity, writing them directly in terms of the static geometric configuration. The experimental results shown in Section 3.1 gives support to such assumption and, in this context, the only source of non-linearity is the damping term. However, this parcel will be written in the 'linear' form

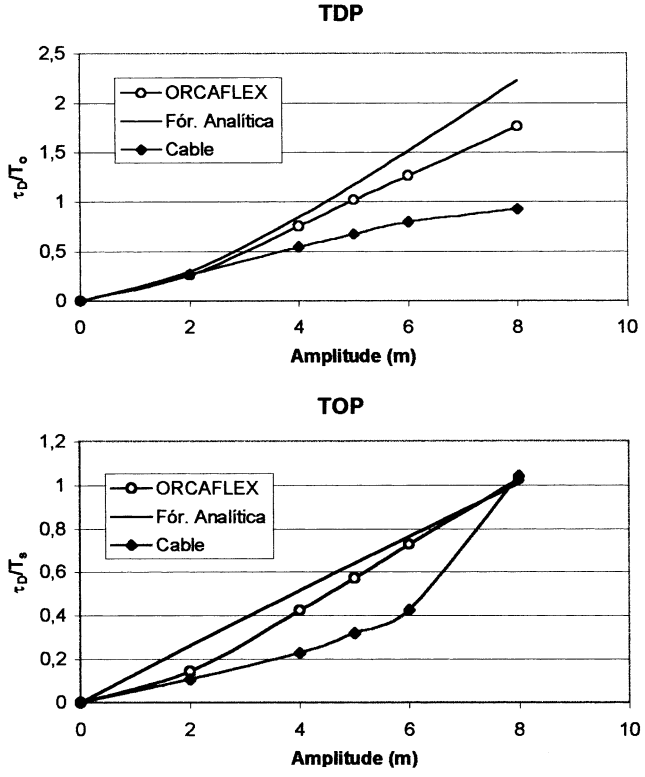

Fig. 9. Dynamic tension at the TOP and TDP as a function of amplitude. *Heterogeneous Line.* ($\theta_S = 58.5°$; $P = 10$ s; w/o current): (—) Eqs. (2.8a)–(2.8c); (-○-) Orcaflex; (-◆-) Cable. (Note: Cable and Orcaflex are coincidents at $A = 2$ m, TDP).

$$d_L(s,t) = -\zeta(m + m_a)\omega\frac{\partial\hat{v}}{\partial t}(s,t), \tag{4.1a}$$

a proper definition for the *nonlinear* ζ will be given later in Section 4.2. Then, the dynamic variables should satisfy the set of *linear* equations (see Ref. [2])

$$\begin{aligned}
&m\frac{\partial^2\hat{u}}{\partial t^2}(s,t) = \frac{\partial\hat{T}_D}{\partial s}(s,t) - T(s)\frac{d\theta}{ds}(s)\,\hat{\varphi}(s,t),\\
&(m + m_a)\left[\frac{\partial^2\hat{v}}{\partial t^2}(s,t) + \zeta\omega\frac{\partial\hat{v}}{\partial t}(s,t)\right]\\
&\quad = \frac{d\theta}{ds}(s)\,\hat{T}_D(s,t) + \frac{\partial}{\partial s}(T(s)\,\hat{\varphi}(s,t)),\\
&\frac{\hat{T}_D(s,t)}{EA} = \frac{\partial\hat{u}}{\partial s}(s,t) - \frac{d\theta}{ds}(s)\,\hat{v}(s,t),\\
&\hat{\varphi}(s,t) = \frac{\partial\hat{v}}{\partial s}(s,t) + \frac{d\theta}{ds}(s)\cdot\hat{u}(s,t),
\end{aligned} \tag{4.1b}$$

subjected to the following boundary conditions:

$$\begin{aligned}
&\hat{u}(l,t) = U_0\cdot e^{i\omega t}, \qquad &&\hat{v}(l,t) = V_0\cdot e^{i\omega t},\\
&\hat{u}(-l',t) = 0, \qquad &&\hat{v}(0,t) = 0.
\end{aligned} \tag{4.1c}$$

In Eq. (4.1c) U_0 and V_0 are the amplitudes of the imposed motion at the suspended end, in the axial and normal

directions respectively, and the boundary conditions at the sea floor deserve some further comments. In fact, although the actual position of the instantaneous touchdown point is of vital importance in the fatigue analysis of risers, see Ref. [3], it can be shown, in first approximation, that the transversal displacement can be taken zero at the *static* touchdown point, as implied by Eq. (4.1c); more is going to be said about the touchdown displacement at the end of Section 4.3. Also, if there is no friction with the sea floor, the axial displacement would be zero at the anchor A placed at $s = -\Delta l$; in the presence of a friction the *static* axial displacement is zero for $s < -l'$, with l' defined in Eq. (2.1b). One can say that the *effective anchor position* in the *static* problem is at $s = -l'$ and this position must be preserved in the geometrically linear dynamic problem; this explains the boundary condition for the axial displacement at the sea floor. Expressing the linear harmonic solution of Eqs. (4.1a)–(4.1c) in the form

$$\{\hat{u}(s,t);\hat{v}(s,t);\hat{\varphi}(s,t);\hat{T}_{\mathrm{D}}(s,t)\} = \{u(\bar{s});v(\bar{s});\varphi(\bar{s});T_{\mathrm{D}}(\bar{s})\}\cdot \mathrm{e}^{\mathrm{i}\omega t},$$
$$\bar{s} = \frac{s}{l}, \tag{4.2a}$$

and introducing the non dimensional variables (see Eqs. (2.7a) and (2.7b) for the definition of σ_{U}, a and T_{e})

$$\tau_{\mathrm{D}}(s) = \frac{T_{\mathrm{D}}(s)}{T_{\mathrm{e}}}, \qquad \epsilon(s) = \frac{T(s)}{\mathrm{EA}},$$
$$\bar{u}(s) = \frac{u(s)}{\sigma_{\mathrm{U}}}, \qquad \bar{v}(s) = \frac{v(s)}{\sigma_{\mathrm{U}}}, \tag{4.2b}$$

the dynamic equation reads (see also Eq. (2.6))

$$-\pi^2\left(\frac{l}{l+l'}\right)^2\left(\frac{\omega}{\omega_{\mathrm{e}}}\right)^2\bar{u}(\bar{s}) = \frac{\mathrm{d}}{\mathrm{d}\bar{s}}\left(\frac{\mathrm{d}\bar{u}}{\mathrm{d}\bar{s}} - \frac{\mathrm{d}\theta}{\mathrm{d}\bar{s}}\cdot\bar{v}\right) - \epsilon(\bar{s})\frac{\mathrm{d}\theta}{\mathrm{d}\bar{s}}\left(\frac{\mathrm{d}\bar{v}}{\mathrm{d}\bar{s}} - \frac{\mathrm{d}\theta}{\mathrm{d}\bar{s}}\cdot\bar{u}\right),$$

$$(-1+\mathrm{i}\zeta)\pi^2\left(\frac{\omega}{\omega_{\mathrm{c}}}\right)^2\bar{v}(\bar{s}) = \frac{\mathrm{EA}}{T_{\mathrm{S}}}\left\{\frac{l}{l+l'}\frac{\mathrm{d}\theta}{\mathrm{d}\bar{s}}\cdot\tau_{\mathrm{D}}(\bar{s}) + \frac{\mathrm{d}}{\mathrm{d}\bar{s}}\left[\epsilon(\bar{s})\left(\frac{\mathrm{d}\bar{v}}{\mathrm{d}\bar{s}} - \frac{\mathrm{d}\theta}{\mathrm{d}\bar{s}}\cdot\bar{u}(\bar{s})\right)\right]\right\},$$

$$\tau_{\mathrm{D}}(\bar{s}) = \frac{l+l'}{l}\left(\frac{\mathrm{d}\bar{u}}{\mathrm{d}\bar{s}} - \frac{\mathrm{d}\theta}{\mathrm{d}\bar{s}}\cdot\bar{v}\right), \tag{4.2c}$$

with

$$\bar{u}(l) = a, \qquad \bar{v}(l) = (V_0/U_0)a,$$
$$\bar{u}(-l'/l) = 0, \qquad \bar{v}(0) = 0. \tag{4.2d}$$

The asymptotic solution of Eqs. (4.2c) and (4.2d) will be elaborated next.

4.1. Asymptotic solution

If the term proportional to the static deformation $\epsilon(s)$ is ignored in the axial equilibrium equation one obtains, after a further derivation with respect to s, that

$$\left(\frac{l+l'}{l}\right)^2\frac{\mathrm{d}^2}{\mathrm{d}\bar{s}^2}\left(\frac{\mathrm{d}\bar{u}}{\mathrm{d}\bar{s}} - \frac{\mathrm{d}\theta}{\mathrm{d}\bar{s}}\cdot\bar{v}\right) = -\pi^2\left(\frac{\omega}{\omega_{\mathrm{e}}}\right)^2\frac{\mathrm{d}\bar{u}}{\mathrm{d}\bar{s}}$$
$$= -\pi^2\left(\frac{\omega}{\omega_{\mathrm{e}}}\right)^2\left(\frac{\mathrm{d}\bar{u}}{\mathrm{d}\bar{s}} - \frac{\mathrm{d}\theta}{\mathrm{d}\bar{s}}\cdot\bar{v}\right) - \pi^2\left(\frac{\omega}{\omega_{\mathrm{e}}}\right)^2\frac{\mathrm{d}\theta}{\mathrm{d}\bar{s}}\cdot\bar{v},$$

and so

$$\frac{\mathrm{d}^2\tau_{\mathrm{D}}}{\mathrm{d}\bar{s}} + \pi^2\left(\frac{l}{l+l'}\right)^2\left(\frac{\omega}{\omega_{\mathrm{e}}}\right)^2\tau_{\mathrm{D}}$$
$$= -\frac{l}{l+l'}\pi^2\left(\frac{\omega}{\omega_{\mathrm{e}}}\right)^2\frac{\mathrm{d}\theta}{\mathrm{d}s}(\bar{s})\cdot\bar{v}(\bar{s}).$$

If now $(\omega/\omega_{\mathrm{e}})^2$ is disregarded when compared to 1 in the left hand side of the above equation[6] then, with an error of the form $[1 + O(\epsilon;(\omega/\omega_{\mathrm{e}})^2)]$, one has

$$\frac{\mathrm{d}^2\tau_{\mathrm{D}}}{\mathrm{d}\bar{s}^2} \cong -\frac{l}{l+l'}\pi^2\left(\frac{\omega}{\omega_{\mathrm{e}}}\right)^2\frac{\mathrm{d}\theta}{\mathrm{d}\bar{s}}(\bar{s})\cdot\bar{v}(\bar{s}).$$

On the sea floor, where $\theta(s) \equiv 0$, the dynamic tension is constant, see Eq. (4.2c), and so $\mathrm{d}\tau_{\mathrm{D}}/\mathrm{d}s = 0$ for $-l' \le s \le 0$; ifthe above equality is integrated from $s = -l'$ to $s = l$, the following expression is obtained for the derivative of the dynamic tension at the suspended end:

$$\frac{\mathrm{d}\tau_{\mathrm{D}}}{\mathrm{d}\bar{s}^2}(1) = -\frac{l}{l+l'}\pi^2\left(\frac{\omega}{\omega_{\mathrm{e}}}\right)^2\int_0^1\frac{\mathrm{d}\theta}{\mathrm{d}\bar{s}}(\bar{s})\cdot\bar{v}(\bar{s})\,\mathrm{d}\bar{s}.$$

The variation of the dynamic tension along the suspended length is weak, once it is proportional to $(\omega/\omega_{\mathrm{e}})^2$, and it can be assumed of the form

$$\tau_{\mathrm{D}}(\bar{s}) \cong \tau_{\mathrm{D}}(0) + \tfrac{1}{2}(1+\sin al\,\bar{s})\cdot[\tau_{\mathrm{D}}(1) - \tau_{\mathrm{D}}(0)]\cdot\bar{s}, \tag{4.3a}$$

with

$$[\tau_{\mathrm{D}}(l) - \tau_{\mathrm{D}}(0)] = -\frac{l}{l+l'}\pi^2\left(\frac{\omega}{\omega_{\mathrm{e}}}\right)^2\int_0^1\frac{\mathrm{d}\theta}{\mathrm{d}\bar{s}}(\bar{s})\cdot\bar{v}(\bar{s})\,\mathrm{d}\bar{s}. \tag{4.3b}$$

Now consider the equilibrium Eq. (4.2c) in the transversal direction, disregarding again the term proportional to $\epsilon(s)$. The error in this approximation will be analyzed in Section 4.3 of this section but one point should be observed here: the higher order derivative in the transversal equation is lost in this approximation and, with it, the imposed boundary conditions on $v(s)$; as it is usual, this gives rise to a *boundary layer* correction near the extremities, briefly elaborated in

[6] Recall that the variation of τ_{D} along the suspended length has a *relative* importance only when $\tau_{\mathrm{D}} \ll 1$; if $\tau_{\mathrm{D}} \cong \mathrm{O}(1)$ this variation is of secondary importance since it is of order $(\omega/\omega_{\mathrm{e}})^2 \ll 1$, see Eq. (4.3b).

Section 4.3. Ignoring here these localized corrections one has

$$(-1+\mathrm{i}\zeta)\pi^2\left(\frac{\omega}{\omega_c}\right)^2\bar{v}(\bar{s})$$

$$=\frac{EA}{T_S}\frac{l}{l+l'}\frac{d\theta}{d\bar{s}}\left[\tau_D(0)+\tfrac{1}{2}(1+\sin al\,\bar{s})\cdot(\tau_D(1)-\tau_D(0))\cdot\bar{s}\right].$$

The parcel $(\tau_D(1)-\tau_D(0))$ is of order $(\omega/\omega_e)^2 \ll 1$ and it becomes relevant only when the dynamic tension $\tau_D(0)$ is also very small. As seen at the end of Section 2, this situation occurs for a 'vertical cable' ($\theta_S \approx \pi/2$), where $\tau_D \ll 1$ since $\Lambda \gg 1$. However, in this case the term $d\theta/ds(\tau_D(1)-\tau_D(0))\cdot s/l$ in the above expression can be ignored by a geometric argument: for a vertical cable the curvature $d\theta/ds$ is appreciable only in the vicinity of the touchdown point, where then $s/l \ll 1$. For a 'non vertical cable' the parameter Λ decreases and the dynamic tension increases, turning irrelevant the correction proportional to $(\tau_D(1)-\tau_D(0))$. As a conclusion, one has, with the help of Eqs. (2.2a), (2.3c) and (2.7c), that the transversal equilibrium equation reduces to

$$(-1+\mathrm{i}\zeta)\Omega^2\bar{v}(\bar{s}) \cong \frac{T_S}{ql}\frac{1}{I_2}\cdot\chi_1(\bar{s})\cdot\tau_D(0). \tag{4.4a}$$

Expression (4.4a) indicates that, in first approximation, the transversal displacement is proportional to the static curvature and thus

$$\bar{v}(\bar{s}) \cong \frac{T_S}{ql}\cdot\frac{1}{I_2}\cdot aV_T\cdot\chi_1(s), \tag{4.4b}$$

With V_T being the *non dimensional amplitude* of the lateral displacement. Notice that Eq. (4.4b) must be corrected at the small boundary layers near the extremities but these corrections have a small integral contribution for the overall equilibrium of the cable. Placing Eq. (4.4b) into Eq. (4.4a) one obtains the algebraic relation

$$(-1+\mathrm{i}\zeta)\Omega^2 V_T = \frac{\tau_D(0)}{a}. \tag{4.4c}$$

A second relation can be obtained from the integration of the expression that defines $\tau_D(s)$ in Eq. (4.2c); in fact, from this expression and Eqs. (4.3a) and (4.3b) it follows that

$$\int_{-l'/l}^{1}\tau_D(\bar{s})\,d\bar{s}$$

$$=\frac{l+l'}{l}\left[\tau_D(0)-\frac{1}{2}\pi^2\left(\frac{l}{l+l'}\frac{\omega}{\omega_e}\right)^2\int_0^1\frac{d\theta}{d\bar{s}}(\bar{s})v(\bar{s})\,d\bar{s}\right]$$

$$=\frac{l+l'}{l}\left[a-\int_0^1\frac{d\theta}{d\bar{s}}(\bar{s})v(\bar{s})\,d\bar{s}\right].$$

where the boundary conditions for the axial displacement $u(s)$ have been used. With an error of the form $[1+O((\omega/\omega_e)^2)]$

$$\frac{\tau_D(0)}{a} = 1 - V_T. \tag{4.4d}$$

From Eq. (4.3b) it also follows that

$$\frac{1}{a}[\tau_D(1)-\tau_D(0)] = -\frac{l}{l+l'}\pi^2\left(\frac{\omega}{\omega_e}\right)^2 V_T$$

$$=-\frac{l}{l+l'}\pi^2\left(\frac{\omega}{\omega_e}\right)^2\left(1-\frac{\tau_D(0)}{a}\right),$$

and again the same argument can be used: the variation of the dynamic tension along the suspended length has a relative importance only when $\tau_D(0) \ll 1$ and, in this case, one has

$$\frac{1}{a}[\tau_D(1)-\tau_D(0)] \cong -\frac{l}{l+l'}\pi^2\left(\frac{\omega}{\omega_e}\right)^2.$$

Now, if the damping factor ζ is given, the non dimensional amplitude V_T and the normalized dynamic tension at the tuchdown point $\tau_D(0)$ can be determined from the solution of the algebraic system Eqs. (4.4c) and (4.4d); the dynamic tension $\tau_D(s)$ along the cable is

$$\tau_D(s) = \tau_D(0) - a\frac{l}{l+l'}\pi^2\left(\frac{\omega}{\omega_e}\right)^2\frac{s}{l}, \qquad 0 \le s \le l. \tag{4.5}$$

A proper definition for the damping factor ζ will be elaborated next.

4.2. A model for the viscous damping

The viscous drag force in the *dynamic problem* is given by the known expression

$$d_v(s,t) = \frac{1}{2}\rho C_D D\left|V_c(s)\sin\theta(s) - \frac{\partial\hat{v}}{\partial t}(s,t)\right|$$

$$\times\left(V_c(s)\sin\theta(s) - \frac{\partial\hat{v}}{\partial t}(s,t)\right)$$

$$-\frac{1}{2}\rho C_D D|V_c(s)\sin\theta(s)|V_c(s)\sin\theta(s), \tag{4.6a}$$

Where $V_c(s)$ is the projection of the horizontal ocean current on the cable's plane. On the other hand, the dissipative force was assumed, in this section, in form Eq. (4.1a) and the two expressions can be related by imposing the equality of the dissipated power in one cycle, namely

$$\frac{l}{l}\int_0^l\left\langle d_V(s,t)\cdot\frac{\partial\hat{v}}{\partial t}(s,t)\right\rangle ds = \frac{l}{l}\int_0^l\left\langle d_L(s,t)\cdot\frac{\partial\hat{v}}{\partial t}(s,t)\right\rangle ds,$$

$$\langle f(t)\rangle = \frac{\omega}{2\pi}\int_0^{2\pi/\omega} f(t)dt.$$

Placing Eq. (4.1a) in the above integral, using Eqs. (4.2b)

and (4.4b) and the definition (2.3a), the following relation can be derived

$$\frac{l}{l}\int_0^l \left\langle d_V(s,t)\cdot\frac{\partial \hat{v}}{\partial t}(s,t)\right\rangle ds = -\tfrac{1}{2}\zeta(m+m_a)\omega^3\left(\frac{T_S}{ql}\frac{1}{I_2}a\sigma_U|V_T|\right)^2 I_2. \tag{4.6b}$$

If $V_c(s)\equiv 0$ one obtains

$$\frac{l}{l}\int_0^l \left\langle d_v(s,t)\cdot\frac{\partial \hat{v}}{\partial t}(s,t)\right\rangle ds = -\frac{2}{3\pi}\rho C_D D\omega^3\left(\frac{T_S}{ql}\frac{1}{I_2}a\sigma_U|V_T|\right)^3 I_3,$$

and then

$$\zeta = a|V_T|\zeta_0, \qquad \zeta_0 = \frac{8}{3\pi}\frac{2C_D}{\pi}\cdot\frac{\rho\pi D^2/4}{m+m_a}\frac{T_S}{ql}\frac{I_3}{I_2^2}\frac{\sigma_U}{D}. \tag{4.7a}$$

In the other hand, for a *strong current*, when $V_c\sin\theta(s) > \partial\hat{v}/\partial t$, one has

$$\frac{l}{l}\int_0^1 \left\langle d_V(s,t)\cdot\frac{\partial \hat{v}}{\partial t}(s,t)\right\rangle ds = -\tfrac{1}{2}\rho C_D D V_c\omega^2\left(\frac{T_S}{ql}\frac{1}{I_2}a\sigma_U|V_T|\right)^2 I_c,$$

and so

$$\zeta = \zeta_c, \qquad \zeta_c = \frac{2C_D}{\pi}\frac{\rho\pi D^2/4}{m+m_a}\frac{2V_c}{\omega D}\frac{I_c}{I_2}. \tag{4.7b}$$

For a *moderated current* the relative velocity in Eq. (4.6a) becomes negative in part of the cycle and the expression for ζ is obviously more complicated; to preserve the simplicity, the following definition for the damping coefficient was assumed in this work

$$\zeta = \sqrt{(a|V_T|\zeta_0)^2 + (\zeta_c)^2}. \tag{4.7c}$$

Notice here that since, in general, one has $\{U_0/D; 2V_c/\omega D\} \gg 1$ therefore, in general, one must have $\zeta \gg 1$: in short, the viscous damping is *super critical* in the cable's dynamic. Placing now Eq. (4.7c) into Eq. (4.4c) and solving the system (4.4c) and (4.4d) one obtains

$$|V_T| = \frac{1/\Omega^2}{\sqrt{\left(\frac{1-\Omega^2}{\Omega^2}\right)^2+\zeta^2}},$$

showing that in fact the cable *freezes* ($|V_T|\to 0$) when either ω or U_0 (see expression for ζ_0) increases; using this value for $|V_T|$ in Eq. (4.7c) the following expression for the damping coefficient is obtained:

$$\zeta^2 = \frac{1}{2}\sqrt{\left(\left(\frac{1-\Omega^2}{\Omega^2}\right)^2+\zeta_c^2\right)^2+\frac{4\zeta_0^2}{\Omega^4}a^2} + \frac{1}{2}\left(\zeta_c^2-\left(\frac{1-\Omega^2}{\Omega^2}\right)^2\right). \tag{4.8}$$

With Eq. (4.8) the system (4.4c) and (4.4d) can be solved and, after some algebra, the result (2.8a)–(2.8c) is obtained.

4.3. Quasi-static solution and boundary layers

As has already been seen, the error in the approximation for the axial equation is of the form $[1 + O(\epsilon(s); (\omega/\omega_e)^2)]$ and the intension now is to assess the error in the approximation for the transversal equation. When $\tau_D(s) \cong O(1)$ the error is, indeed, of this same order of magnitude; however, when $\Omega^2 \ll 1$ one has, as seen at the end of Section 2, that $\tau_D(s) \cong O(\Omega^2)$ and the error in this approximtion must be reevaluated. In this case the approximation used is correct if and only if

$$\underbrace{\frac{d\theta}{d\bar{s}}}_{ql/T_S}\cdot\underbrace{\tau_D}_{\Omega^2} \gg \underbrace{\epsilon(\bar{s})}_{T_S/EA}\cdot\underbrace{\bar{v}(\bar{s})}_{T_S/ql}$$

or (see Eq. (2.3c))

$$\Omega^2 \gg \left(\frac{T_S}{ql}\right)^2\frac{T_S}{EA} \cong O\left(\frac{1}{\Lambda^2}\right).$$

It follows then that the proposed dynamic approximation is valid when $\Omega^2 \ll 1$ if and only if the inequality

$$\pi^2\left(\frac{\omega}{\omega_C}\right)^2 \gg 1\left(\text{or } \tau_D \cong O(\Omega^2) \gg \frac{1}{\Lambda^2}\right) \tag{4.9a}$$

is satisfied simultaneously. In otherwords: when

$$\frac{\omega}{\omega_C} \le O(1/\pi) \tag{4.9b}$$

the proposed approximation is not valid anymore but the *response is quasi-static* then.

This solution is elaborated in Ref. [2] and only the final answer wil be presented here; in this way, if $\theta(s) = (ql/T_S)\chi_0(s)$ and the integrals

$$J_n = \frac{1}{l}\int_0^l \frac{\chi_0^n}{T(s)/T_S}ds, \qquad n = 0,1,2, \tag{4.10a}$$

are defined, the quasi static solution is given by

$$\tau_{QE} = a\cdot\frac{\left|1-\frac{V_0}{U_0}\left[\theta(l)-\frac{ql}{T_S}\frac{J_1}{J_2}\right]\right|}{1+\left[J_2-\frac{J_1^2}{J_0}\right]\cdot\frac{\Lambda^2}{I_2}}. \tag{4.10b}$$

This result is consistent with Eq. (4.9a): since $J_2 - J_1^2/J_0 > 0$, then $\tau_{QE} \cong O(1/\Lambda^2)$, showing that the dynamic result (2.8a)–(2.8c) diminishes with Ω^2 until the level $O(1/\Lambda^2)$ is reached, when then one should switch to the quasi-static solution. To make the analysis simpler the following rule was used to plot the theoretical curve in Fig. 1a: if $\tau_{(2.8)} > \tau_{QE}$ then the value $\tau_D(0) = \tau_{(2.8)}$ was taken; if $\tau_{(2.8)} < \tau_{QE}$ then $\tau_D(0) = \tau_{QE}$. The experimental results confirm the adequacy of such simple strategy.

Finally, the question of the transversal boundary condition (4.1c), lost in the dynamic approximation (2.8a)–(2.8c), will be briefly addressed. To make more direct the exposition more straightforward, the boundary layer in the vicnity of the *touchdown point* will be worked out below. In this case the transversal Eq. (4.2c) is reduced to ($s \cong 0$)

$$\frac{T_0}{T_S}\frac{d^2\bar{v}}{d\bar{s}^2} + (1 - i\zeta)\pi^2\left(\frac{\omega}{\omega_C}\right)^2\bar{v} = -\frac{EA}{T_S}\frac{l}{l+l'}\frac{d\theta}{d\bar{s}}(0)\,\tau_D(0). \tag{4.11a}$$

Introducing the parameter p by the expression

$$1 - i\zeta = \sqrt{1+\zeta^2}\cdot e^{-i\Psi},$$
$$p = \sqrt{\frac{T_S}{T_0}(1+\zeta^2)^{1/2}}\cdot\pi\left(\frac{\omega}{\omega_C}\right)\cdot e^{-i\Psi/2}; |p| \gg 1, \tag{4.11b}$$

then Eq. (4.4b) is, in the jargon of the boundary layer theory, an *outer solution* of Eq. (4.11a) with an error of order $O(1/p^2)$, see Ref. [4]; obviously Eq. (4.4b) is a *particular solution* of the linear Eq. (4.11a), the total solution, satisfying the boundary condition $v(0) = 0$, being given by

$$\bar{v}(\bar{s}) = \frac{T_S}{ql}\frac{1}{I_2}aV_T[\chi_1(\bar{s}) - \chi_1(0)\cdot e^{-p\bar{s}}]. \tag{4.11c}$$

The dynamic angular displacement at the static touchdown point is equal to

$$\varphi(0) = \frac{\sigma_U}{l}\frac{d\bar{v}}{d\bar{s}}(0) = \frac{\sigma_U}{l}\frac{T_S}{ql}\frac{1}{I_2}aV_T\left[\frac{d\chi_1}{d\bar{s}}(0) + p\chi_1(0)\right], \tag{4.12a}$$

and, as shown in Ref. [3], if the instantaneous touchdown point is at $s = X(t)$ one must have $\theta(X(t)) + \varphi(0)\cdot e^{i\omega t} \equiv 0$. Since $\{\theta(0) = 0; d\theta/ds(0) = q/T_0\}$ then, if $X(t) = X_0\cdot e^{i\omega t}$, the amplitude X_0 of the horizontal displacement of the touchdown point can be approximated by the expression

$$\frac{X_0}{l} \cong -\frac{T_0}{ql}\varphi(0)$$
$$\cong -\frac{\sigma_U}{l}\cdot\frac{T_0}{T_S}\left(\frac{T_S}{ql}\right)^2\frac{1}{I_2}aV_T\left[\frac{d\chi_1}{d\bar{s}}(0) + p\chi_1(0)\right]. \tag{4.12b}$$

In the fatigue induced by the cyclic variation of the curvature at the touchdown, the motion of this point, and thus the amplitude X_0, is of crucial importance. The cyclic variation of the curvature, obtained in Ref. [3], compares well with some experiments, as discussed in Ref. [8], and Eq. (4.12b) makes possible to estimate this variation analytically.

At the suspended end a similar analysis can be pursued and the boundary condition $v(l) = V_0$ can then be imposed. Also, in a *heterogeneous* cable the curvature is discontinuous when $q(s)$ is and boundary layers occur at these discontinuity points. Again, these local corrections do not affect the overall dynamics of the cable and are of little practical importance.

References

[1] Andrade BLR. Estudo experimental do comportamento dinâmico de linhas de amarração, Tese de Mestrado, Departmento de Engenharia Naval e Oceânica, EPUSP, 1993.

[2] Aranha JAP, Pesce CP, Martins CA, Andrade BLR. Mechanics of submerged cables: asymptotic solution for the dynamic tension. Polar Engineers, ISOPE-93, Singapore, 6–11 June, 1993.

[3] Aranha JAP, Martins CA, Pesce CP. Analytical approximation for the dynamic bending moment at the touchdown point of a catenary riser. Int J Offshore Polar Engng 1997;7(4):229–300.

[4] Bender C, Orzag S. Advanced mathematical methods for Scientist and Engineers. New York: McGraw-Hill, 1978.

[5] Howell CT. Investigation of the Dynamics of Low Tension Cables. PhD Thesis. Ocean Engineering Department, MIT, 1992.

[6] Irvine HM, Caughey TK. The linear theory of the free vibration of a suspended cable. Phil Trans R Soc Lond A 1974;341:229–315.

[7] Larsen CM. Flexible riser analysis: comparison of results from computer programs. Mar Struct 1992;5(5):103–19 (special issue on flexible risers (Part 1)).

[8] Pesce CP, Aranha JAP, Martins CA, Ricardo OGS, Silva S. Dynamic curvature in catenary risers at the touchdown region: an experimental study and the analytical boundary layer solution. Int J Offshore Polar Engng 1998;8(4):303–10.

[9] Triantafyllou MS, Bliek A, Shin H. Dynamic analysis as a tool for open-sea mooring system design, presented at the Annual Meeting of the Society of Naval Architects and Marine Engineers, New York, 1985.